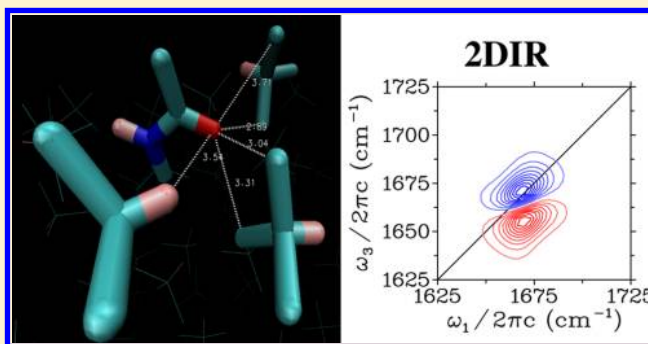


Linear Absorption and Two-Dimensional Infrared Spectra of *N*-Methylacetamide in Chloroform Revisited: Polarizability and Multipole Effects

Thomas L. C. Jansen*

Zernike Institute for Advanced Materials, University of Groningen, Nijenborgh 4, 9747 AG Groningen, The Netherlands

ABSTRACT: The effect of solvent polarizability and multipole effects on the amide I vibrational spectra of a peptide unit is investigated. Four molecular dynamics force fields of increasing complexity for the solvent are used to model both the linear absorption and two-dimensional infrared spectra. It is observed that, at least in chloroform solution, the predicted solvent shift is considerably improved when accounting for the polarizability and multipole effects. The latter are typically connected with halogen bonding. Significant deviations are still observed for more sensitive line shape parameters such as the spectral width and line skewness. However, the findings demonstrate that previously observed deviations have an origin in the force field treatment rather than in the electrostatic mapping procedure frequently employed to simulate linear absorption and two-dimensional infrared spectroscopy.



INTRODUCTION

Two-dimensional infrared (2DIR) spectroscopy in the amide I region (CO stretch) has emerged as a powerful tool for determining the structure of peptides and proteins.^{1,2} Different structural elements such as α -helices, β -sheets, and 3_{10} helices give rise to distinctively different lineshapes.^{3–5} In combination with isotope labeling techniques, information about, for example, local structure and solvent exposure can be determined.^{6–14} The interpretation of the spectra greatly relies on theoretical support. Molecular dynamics (MD) force fields and specially developed frequency mappings are crucial elements for the spectral simulations. Great successes in the modeling of the spectra have been seen; however, a few specific cases do raise concern about how well force fields¹⁵ and mappings¹⁶ can be trusted. In this paper the particular case of deuterated *N*-methylacetamide (NMA-*d*) in deuterated chloroform (CDCl₃)^{16–18} will be revisited. NMA-*d* is a model molecule for the protein backbone building blocks, and the previous simulations of NMA-*d* in chloroform have shown very large deviations from experimental observations.^{17,18}

Numerous force fields exist for peptides and proteins^{15,19–21} and solvents.^{22–25} These are usually parametrized and tested on averaged properties such as densities, diffusion constants, vaporization energies, and dielectric constants. However, tests on more complex quantities such as nuclear magnetic resonance measurements are less common.¹⁹ For the chloroform solvent that we will consider here, both point charge,²³ polarizable force fields,^{26,27} and recently polarizable multipole force fields²⁸ are known. For consistency, we will here consider force fields based on the optimized potentials for liquid simulations (OPLS) force field,²³ but add polarizability and

atomic dipoles to investigate their impact on the spectra. This was inspired by recent work on halogen bonding^{29–31} demonstrating that the polarizability and atomic dipoles are crucial for molecular interactions in systems including halogen atoms such as chlorine. One may think that as proteins are usually located either in an aqueous environment or in lipid membranes, interactions with halogen atoms should be esoteric and of little importance. However, protein-binding ligands, including drugs, often contain halogen atoms and halogen bonding is involved in the observed binding mechanisms.^{28,30,31}

Electrostatic mappings to extract the amide I frequency and transition dipole fluctuations from MD trajectories were developed by multiple groups. Many different mapping strategies were employed. In the first mappings for amide I, the frequency was related to the electrostatic potential at different locations of the molecule.^{32,33} Other groups used the electric fields^{16,34–36} or even included electric field gradients.^{18,37,38} For most mappings the parameters were fitted with charges from a specific force field using electronic structure calculations to obtain the frequencies or empirically by fitting to experimental spectra.^{16,35,36} An alternative approach used fixed point charges and electronic structure calculations formally resulting in transferable force field independent mappings.^{18,37,38} The advantage of the former empirical approach is that inaccuracies in the particular force

Special Issue: James L. Skinner Festschrift

Received: February 4, 2014

Revised: March 22, 2014

field and effects not arising directly from the solvent charges may be compensated in the mapping parameters. In the latter approach, only the solvent shift induced by the electric field of the solvent will be included, allowing a more clean interpretation but leaving out effects such as charge-transfer-induced solvent shift.³⁹ In the present study we will apply the transferable electrostatic mapping including electric fields and gradients developed in our group.¹⁸ Thus, the calculated solvent shifts will be determined by only the electrostatic potential generated on the NMA-*d* molecule. Using the different force fields as discussed above, the effect of polarizability and atomic dipoles will then be tested.

Apart from simulating the commonly known linear absorption spectra, we will simulate the 2DIR spectra. In this type of spectroscopy, the vibration is first excited using one pair of laser pulses and then, following a waiting time, probed by another laser pulse.^{1,2} Using the control of the time delays on the femtosecond time scale one then obtains a two-dimensional correlation spectrum quite similar to that of two-dimensional nuclear magnetic resonance experiments.⁴⁰ In essence, the frequency on one axis provides the frequency of the molecules before the waiting time and the frequency on the other axis provides the frequency of the same molecules after the waiting time. In this way, a diagonally elongated signal reveals that the memory of the molecular environment determining the vibrational frequency was preserved during the waiting time and a round peak discloses that this memory has been lost. Therefore, two-dimensional infrared spectroscopy has a close connection with the frequency autocorrelation function⁴¹ and is a good probe of ultrafast dynamics, which has been applied to study a large range of dynamical phenomena on the femtosecond and picosecond time scales.^{42–51} One can thus expect 2DIR to be sensitive to details of force fields determining the dynamics in MD simulations. In this study we will simulate the 2DIR spectra, the related frequency autocorrelation functions, and polarization anisotropy for the four different force fields and compare the results with experiment to find out how sensitive these spectroscopic observables are to the force field parameters used to simulate them.

MODELING

Typically, infrared spectra for the amide I region of proteins are measured in heavy water to eliminate the signal of the water bend vibration found in the same spectral region. This leads to exchange of all acidic protons in the proteins including the protons in the backbone amide units. Therefore, the experiments were performed on NMA-*d* in deuterated chloroform,¹⁷ and we will use the deuterated species in this study. For NMA-*d*, the GROMOS87 force field parameters^{52–54} used were the same as those used in the original paper.¹⁸

Four force fields were used for CDCl₃: The original united atom point charge OPLS force field,²³ which we will denote UPC. The same force field, but with polarizability added, which we will denote UPO. A polarizable all-atom force field is denoted PO. A force field with polarizability and extra charges at the chlorine atoms mimicking atomic dipoles in the C–Cl bond direction denoted POMP. All force fields used the original Lennard-Jones parameters from the original united atom OPLS force field.²³

The charges for the different sites in the PO and POMP models were derived from the CHELPG charges. These⁵⁵ were determined using ORCA 2.9.1⁵⁶ with the RPBE exchange

correlation functional⁵⁷ and the Ahlrichs-VDZ basis set.⁵⁸ As the CHELPG charges do not fully reproduce the gas phase dipole moment of 1.15 D nor do they perfectly fulfill the symmetry of the molecules, the charges used in the actual MD simulations were adjusted to meet these requirements. The charges for all models and the CHELPG charges are given in Table 1. The polarizability was modeled using three

Table 1. Charges (in Units of e) for the Three Different Chloroform Force Fields and the CHELPG Charges^a

site	UPC	UPO	PO	POMP	CHELPG
C	0.420	0.420	0.010	0.280	0.316
D	0.000	0.000	0.140	0.110	0.148
Cl	−0.140	−0.140	−0.050	0.030	0.048
M	0.000	0.000	0.000	−0.160	−0.203

^aFor the CHELPG charges, the average values are reported for chlorine and the dummy atom site M used to represent the atomic dipole on chlorine.

independent drude particles⁵⁹ placed at the chlorine atoms for the UPO and PO force fields and on the charge sites M, illustrated in Figure 1, for the POMP force field. The

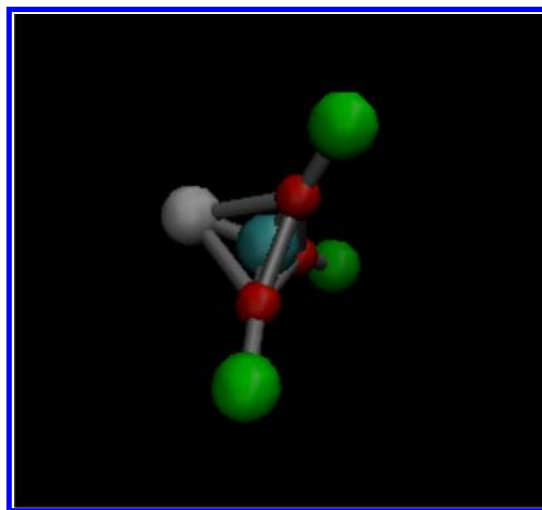


Figure 1. Structure and sites used for the chloroform force field. The C–D distance is 1 Å, the C–Cl distance is 1.76 Å, and the M–Cl distance 1 Å. The atomic colors are carbon (cyan), hydrogen (gray), chlorine (green), and charge centers, M, (red). The drawing was made with VMD.⁸³

polarizability of each drude particle was set to 2.84333 Å³ to reproduce the experimental isotropic molecular polarizability⁶⁰ of 57.56 atomic units. The molecular dipole of chloroform is the same in all the utilized force fields. The density and the self-diffusion constant of bulk deuterated chloroform was calculated using the four force fields. The numbers are reported in Table 2. These properties do vary with the force field parameters, and the POMP force field provides the best agreement with experiment on these bulk properties.

Simulations were performed using simulation boxes with one NMA-*d* molecule and 342 CDCl₃ molecules. One femtosecond time steps were used to generate the final 1 ns trajectories. For the electrostatics, the particle mesh Ewald (PME) summation⁶¹ was employed with a 1.5 nm cutoff identical to that used for the van der Waals interactions. The temperature was kept constant using the Nose–Hoover thermostat⁶² at 300 K, with a coupling

Table 2. Densities and Self-Diffusion Constants (*D*) for Bulk Deuterated Chloroform^a

model	density (g/L)	<i>D</i> (×10 ^{−5} cm ² /s)
UPC	1375	3.8 ± 0.3
UPO	1505	2.2 ± 0.1
PO	1499	2.5 ± 0.1
POMP	1486	2.7 ± 0.01
	exptl	
(CHCl ₃)	1479.5	2.885
(CDCl ₃)	1492	–

^aExperimental data at 25°C are taken from ref 84. The density of CDCl₃ is obtained by simple correction using the isotope weight ratio.

time of 10 ps. For the pressure coupling, the Parrinello–Rahman barostat⁶³ with the compressibility of $4.5 \times 10^{-5} \text{ bar}^{-1}$ and a time scale of 5 ps was employed. All bonds were kept constrained using the LINCS algorithm⁶⁴ mainly to avoid double treatment of the amide I vibrational mode.¹⁸

From the molecular dynamics simulations, the electric fields and electric field gradients on the C, O, N, and D atoms of *N*-methylacetamide were calculated as a function of time. These were translated into Hamiltonian parameters using the electrostatic mapping of ref 18. This mapping provides the fundamental frequency ω , the transition dipole $\vec{\mu}$, the anharmonicity Δ , and the transition dipole for the sequence transition $\vec{\mu}_{12}$. The amide I vibration of the NMA-*d* molecule is then described by the time-dependent Hamiltonian

$$H(t) = \omega(t)B^\dagger B - \frac{\Delta(t)}{2}B^\dagger B^\dagger BB + \vec{E}(t)\vec{\mu}(t)(B^\dagger + B) + \vec{E}(t)\vec{\mu}'(t)(B^\dagger B^\dagger B + B^\dagger BB) \quad (1)$$

Here B^\dagger and B are the usual bosonic creation and annihilation operators and $\vec{E}(t)$ is the laser field applied in the experiments. $\vec{\mu}'(t)$ is the difference between the transition dipole for the sequence transition and that given by the harmonic approximation: $\vec{\mu}'(t) = \vec{\mu}_{12}(t) - \sqrt{2}\vec{\mu}(t)$.⁶⁵

The linear absorption and 2DIR spectra were calculated using the quantum–classical response function formalism^{2,66,67} based on time-dependent perturbation theory using the applied laser pulses as the perturbation.⁶⁸ The simulations were performed using the freely available NISE code.^{69,70} In essence, this required solving the time-dependent Schrödinger equation, which is done by dividing the trajectory into 10 fs time steps (δt) during which the Hamiltonian is assumed to be constant. The time evolution during one time step can then be described by the solution of the time-independent Schrödinger equation providing the time-evolution operators U :

$$U(t + \delta t, t) = \exp\left(-\frac{i}{\hbar}H_0(t)\delta t\right) \quad (2)$$

Here $H_0(t)$ is the perturbation-free Hamiltonian ($\vec{E} = 0$), for which the indicated time-dependence is only parametric in the sense that the Hamiltonian for each time step is different as determined by the molecular dynamics simulation and the electrostatic mapping, whereas it is assumed to be constant during each time step. The time evolution for longer times can then be determined by time-ordered products of the time-evolution operators for individual time steps.

The linear absorption spectra are calculated as the imaginary (absorptive) part of the Fourier transform of the linear response function R ⁶⁸

$$R(\tau_1 - \tau_0) = \frac{i}{\hbar} \langle \mu(\tau_1) U(\tau_1, \tau_0) \mu(\tau_0) \rangle \times \exp(-(\tau_1 - \tau_0)/2T_1) \quad (3)$$

Here the brackets $\langle \dots \rangle$ denote the ensemble average taken by sampling over different starting times τ_0 along the molecular dynamics trajectory. For the present simulations, the used sampling times were separated by 100 fs, resulting in slightly less than 10 000 samples for each spectrum. The response functions were calculated for time differences ($\tau_1 - \tau_0$) from 0 up to 2.56 ps. T_1 is an ad hoc lifetime set to 1.8 ps in all simulations.^{51,71}

The 2DIR spectra were simulated in a very similar way. The response functions governing these spectra are given in ref 69. Again, sampling was performed using starting points separated by 100 fs along the trajectory, resulting in averaging over about 10 000 configurations. For these response functions the delay between the first set of laser pulses, usually denoted t_1 , was varied from 0 to 2.56 ps as was the delay between the last laser pulse and the time of detection, denoted t_3 . To obtain the 2DIR spectra from the response functions, a double Fourier transform was performed with respect to these two times, resulting in two frequency axes, denoted ω_1 and ω_3 for the first and last time delay, respectively. The time between the second and the third laser pulse is denoted the waiting time t_2 . For the POMP force field, waiting times different from zero were simulated as reported later in Results and Discussion. In all other simulations the waiting time was set to zero. All presented spectra were calculated assuming that the polarization of all applied laser pulses were parallel with each other by using the molecular dynamics to lab frame weighting factors given by Hochstrasser.⁷²

The polarization anisotropy is defined as

$$R(t) = \frac{S_{\parallel}(t) - S_{\perp}(t)}{S_{\parallel}(t) + 2S_{\perp}(t)} \quad (4)$$

where S_{\parallel} and S_{\perp} are the two-dimensional signals as a function of waiting times, $t = t_2$, using parallel and perpendicular laser pulse configurations, respectively. In the present simulations, the results were obtained by equating S to the integral over the frequency axes;⁷³ however, this quantity can be analyzed for particular locations in the two-dimensional spectra as well or from traditional pump–probe experiments.⁷⁴ For a single isolated chromophore as studied here the anisotropy will be dominated by the rotational motion of the transition dipole as described by²

$$R(t) = \frac{1}{5} \langle 3|\hat{\mu}(t) \cdot \hat{\mu}(0)|^2 - 1 \rangle \quad (5)$$

The anisotropy will be 0.4 if the transition dipole is not rotating, and it will decay to zero as the orientational correlation is lost during the waiting time of the experiment.

RESULTS AND DISCUSSION

The Cl–O radial distribution functions for the four employed force fields are given in Figure 2. All models display a clear maximum around 0.3 nm. Only the models including polarization display a second maximum at 0.5 nm, which is most pronounced for the POMP force field. A rather flat bump in the radial distribution function is observed for all models around 0.7 nm. The typical halogen bonding distance for the O–Cl halogen bond is about 0.3 nm.²⁸ As all force fields exhibit the first peak at this distance, one could be tempted to conclude

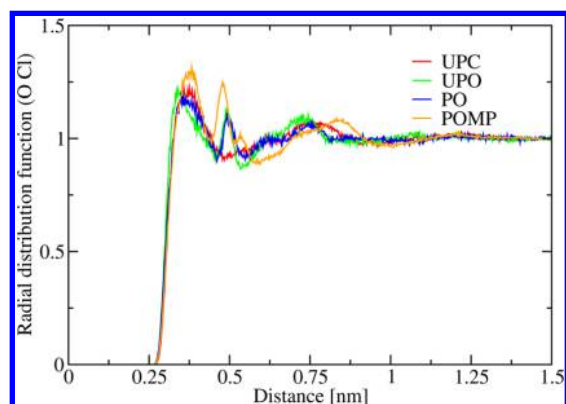


Figure 2. Radial distribution function for the chloroform chlorine to *N*-methylacetamide oxygen atom distance for the four force fields used.

that halogen bonding is present in all cases. However, this distance merely indicates the van der Waals radius of the involved atoms. Halogen bonding is directed, which is rather indicated by the secondary peak arising from local ordering of the nearest chloroform molecules.

The frequency autocorrelation functions for the amide I vibration of the *NMA-d* molecule with the different force fields are given in Figure 3. The frequency autocorrelation functions

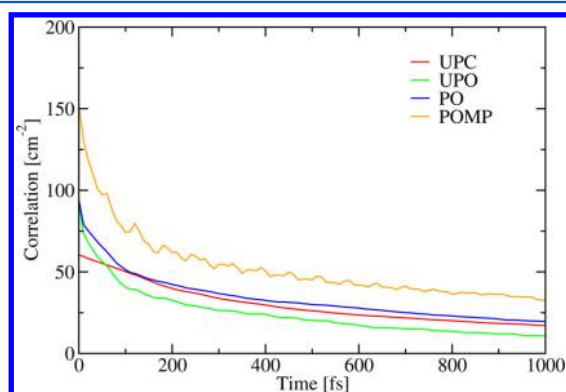


Figure 3. Frequency autocorrelation functions for the amide I vibration of *NMA-d* in the four force fields employed.

were fitted to a biexponential function of the form $C(t) = \sigma_1^2 \exp(-t/T_1) + \sigma_2^2 \exp(-t/T_2)$, and the coefficients are given in Table 3. The polarizable models all have a pronounced fast

Table 3. Coefficients for a Biexponential Fit of the Frequency Autocorrelation Functions

force field	σ_1^2 (cm ⁻²)	T_1 (ps)	σ_2^2 (cm ⁻²)	T_2 (ps)
UPC	35.7	0.26	26.0	2.2
UPO	46.2	0.05	40.9	0.7
PO	41.9	0.06	48.1	1.1
POMP	78.2	0.06	67.3	1.4

contribution with a correlation time around 60 fs, while the fastest component for the UPC model has a correlation time of 260 fs. The slow time scales for the polarizable models are in the range between 700 fs and 1.4 ps. This is faster than that for the UPC force field, where the slow time scale is 2.2 ps. For the POMP force field, a weak set of oscillations similar to those typically observed in hydrogen bonding systems⁷⁵ are seen. This suggests the presence of a low-frequency underdamped

intermolecular vibrational mode, possibly a halogen bond mode. From the 2DIR experiment, three time scales of 4 fs, 620 fs, and 5.6 ps were extracted¹⁷ for the correlation function.

The linear absorption spectra for the four force fields are presented in Figure 4. In Table 4, the peak positions, full width

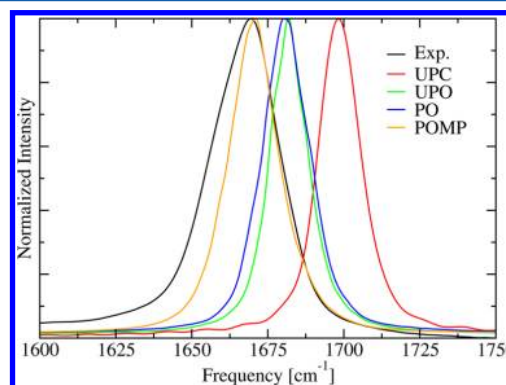


Figure 4. Linear absorption spectra of *NMA-d* for the different force fields compared with experiment.¹⁷

Table 4. Spectral Characteristics for the Four Force Fields Compared with Experiment

property	UPC	UPO	PO	POMP	exptl ¹⁷
peak (cm ⁻¹)	1698	1682	1680	1671	1669
fwhm (cm ⁻¹)	12.3	14.5	18.5	19.2	26.8
skewness (cm ⁻¹)	2.7	0.1	1.3	-0.6	-6.0

at half-maximum (fwhm), and the robust skewness are reported. The robust skewness is defined as the difference between the peak position and the midpoint between the points of the two half maxima. The peak position moves about 15 cm⁻¹ to the red when the polarizability is introduced, while the addition of the explicit hydrogen atom changes the peak position by only 2 cm⁻¹ more. Introducing the atomic dipoles on the chlorine atoms moves the peak 9 cm⁻¹ further to the red, separating it by only about 2 cm⁻¹ from the experimentally observed position. In a similar manner, the peak width increases with the sophistication of the force field, starting with only 12.3 cm⁻¹ for the UPC force field and changing to 19.2 cm⁻¹ for the POMP force field. This is still significantly less than the 26.8 cm⁻¹ fwhm observed in experiment. The robust skewness is positive, corresponding to a tail in the blue side for all force fields except the POMP. While this force field has a negative skewness as in the experiment, the magnitude is considerably underestimated.

The parallel polarization 2DIR spectra for the different force fields are given in Figure 5. The peak positions vary in a way essentially identically to that of the linear absorption spectra. The peak shapes are rather similar for the simulated spectra; even the POMP force field provides the largest elongation along the diagonal direction. Still, both the diagonal and the antidiagonal widths are underestimated in all simulated spectra as compared to those of the experimental spectrum.

In Figure 6 the parallel polarization 2DIR spectra are given for the POMP force field as a function of the waiting time. The elongation along the diagonal is lost on the 2 ps time scale, agreeing well with the correlation time found in the frequency autocorrelation function for this force field. This is faster than the experimental observations¹⁷ and in line with the finding of a longer frequency autocorrelation function component.

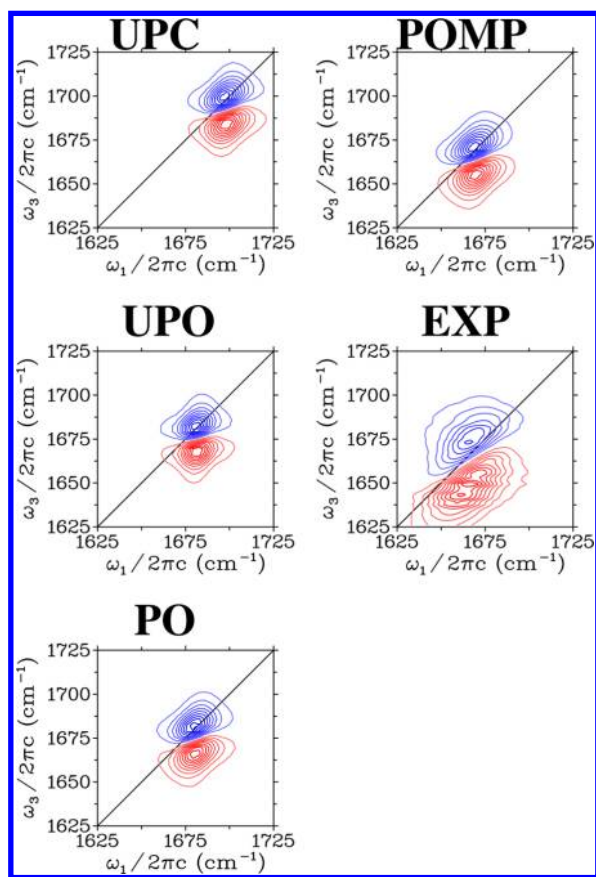


Figure 5. Parallel polarization 2DIR spectra of NMA-*d* in CDCl₃ for the different force fields compared with experiment.¹⁷ The blue contour lines indicate the (negative) bleach signal and the red contour lines indicate the (positive) excited-state absorption signal. Equidistant contour lines were plotted for every 10% of the maximum signal.

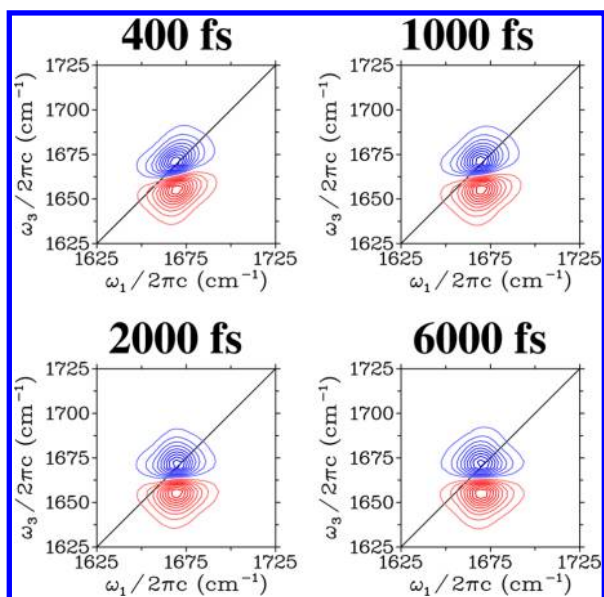


Figure 6. Parallel polarization 2DIR spectra of NMA-*d* in CDCl₃ for the POMP force field as a function of waiting time. The contour lines are drawn as in Figure 5.

The polarization anisotropies for the different force fields are given in Figure 7 along with a biexponential fit to the experimental data as reported in ref 17. The polarizable force

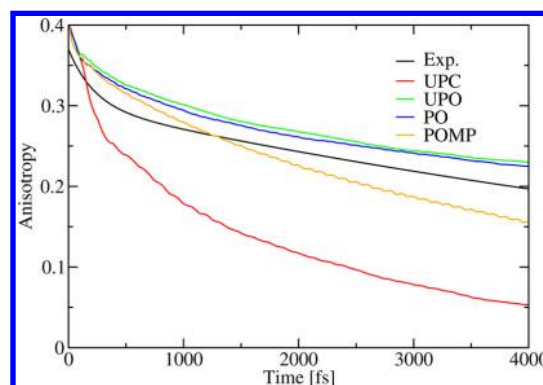


Figure 7. Polarization anisotropy of NMA-*d* for the different force fields compared with a biexponential fit of experimental data.¹⁷

fields clearly give the slowest decay, reflecting slower reorientation correlation times.⁷³ Experimentally, the initial part is typically somewhat affected by the experimental laser pulse duration resulting in anisotropies starting out slightly lower than 0.4. For the longer times, the UPO and PO force fields follow the experimental anisotropy quite well, albeit with a slight offset. Both the POMP and the UPC force fields result in a too fast decay of the anisotropy; however, this is most severe in the UPC force field.

Considering all findings described above, it is clear that both the polarizability and the effect of details of the atomic charge distribution such as the atomic dipoles accounted for here play a significant role. Accounting for these is important, at least for chloroform, which contains large polarizable chlorine atoms. Previous studies considering the effect of the polarizability of water^{49,76,77} on the vibrational spectroscopy of the OH-stretch showed much smaller effects, likely because of the rather small polarizability of water and the fact that standard force fields include this effect in an average way by using a dipole larger than the gas phase one.^{24,25} With the new POMP force field, we managed to account for 46 cm⁻¹ of the experimentally observed 48 cm⁻¹ solvent shift in contrast to the previous simulations accounting for a shift of only 19 cm⁻¹.¹⁸ Other simulations have found a similar underestimation of the solvent shift using similar point-charge-based force fields.¹⁷ The spectral width and skewness is improved by including polarizability and atomic dipoles on chloroform, although these are still both significantly underestimated.

The properties discussed above are all mainly static in character, depending on the electric field distribution generated by the solvent rather than on the solvent dynamics. The 2DIR spectra and the polarization anisotropy reflect the dynamic aspects. Here we found that all force fields including polarizability significantly speed up the components of the frequency autocorrelation function reflected in the spectral shape. The time scales do not match experimental observations particularly well. Specifically, a slow 5.6 ps component is not observed. For the short time behavior it should be noted that the experiment is very sensitive to the finite pulse duration, which was not accounted for in the simulations. The polarization anisotropy became significantly slower by including the polarizability of the solvent molecules, reflecting a slower reorientational correlation time possibly connected with the formation of halogen bonds. The anisotropy found with the polarizable models is in much better agreement with experimental findings than that of the point charge model.

The force fields tested here were constructed in an incremental manner by adding more details in each step, thus allowing an estimate of how important each level of complication is. None of the force fields were particularly optimized to reproduce the spectral observables, and the relatively crude united atom point charge force field for NMA-*d* was retained all through the study to allow a comparison of the solvent force fields. It is thus very likely that the agreement between simulation and experiment can be improved further as compared to that found with the POMP force field. In particular, one could include the polarizability of the NMA-*d* molecule and use the full anisotropic polarizability of the chloroform molecules. The aim of this study, however, was not to optimize the force field but to investigate to what extent the force field description in previous studies is important to the rather large discrepancies previously reported between theory and experiment^{17,18} as compared to approximations in the mapping procedure. Our findings demonstrate that at least for chloroform it makes more sense to optimize the force field than to empirically determine the mapping parameters assuming a particular point charge force field for chloroform, as was recently done.¹⁶ Furthermore, the infrared spectral observables are quite sensitive to the force field parameters and especially to the resulting dynamics, and they may provide a strong additional constraint for force field optimization that typically relies more on static properties as binding energies, radial distribution functions, densities, and dielectric properties.

The present approach assumed that the amide I frequency fluctuations depend solely on the electrostatic interactions as described by the electrostatic mapping. Of course other forces, such as the van der Waal interactions,^{78,79} may play a role, as may charge-transfer-like interactions.^{39,80,81} To utilize vibrational spectroscopic observables for faithful force field fitting the contribution from such alternative sources need to be understood and included if they significantly contribute. The remaining differences with experiment can thus be caused by charge-transfer interactions or van der Waals interactions. Furthermore, it is possible that higher-order multipole interactions contribute and that small adjustment of the presently used parameters, including those of the force field for *N*-methyl acetamide, may improve the agreement between theory and experiment. The present demonstration that improved force fields lead to better spectra may also be applicable to other systems with strong interactions. In particular, interactions involving automatic rings that may participate in π -hydrogen bonding can be insufficiently described by standard force fields. For example, it was demonstrated using ab initio calculation that a π -hydrogen bond between the NH of the amide group with a benzene ring leads to a 10 cm⁻¹ redshift of the amide I vibration.⁸²

CONCLUSIONS

We investigated the effect of increasing force field complexity on the simulated amide I linear absorption and two-dimensional infrared signals. We found that both the polarizability and the atomic dipole on the chlorine atoms contribute significantly to the experimentally observed solvent shift of the amide I vibration in chloroform. It cannot be excluded that other effects neglected in this study, such as the van der Waals interaction induced shifts and charge transfer, contribute to the spectral shape. It is, however, clear that the main contribution to the solvent shift has an electrostatic origin.

The present study demonstrates that for simulating vibrational spectra of the amide I vibration in solution one needs to properly account for the electrostatic environment and that going beyond simple atomic point charge models is required at least for solvent environments containing large, soft atoms such as chlorine. The solvent shift, spectral width, robust spectral skewness, and polarization anisotropy are sensitive to the details of the solute–solvent interaction. Vibrational spectroscopy and in particular two-dimensional infrared spectroscopy will thus be an excellent tool for studying and understanding halogen bonding, just as this tool has previously been utilized to study hydrogen bonding dynamics.

AUTHOR INFORMATION

Corresponding Author

*E-mail: t.l.c.jansen@rug.nl.

Notes

The authors declare no competing financial interest.

ACKNOWLEDGMENTS

Haime Torii and Jim Skinner are kindly acknowledged for helpful discussions, and Andrei Tokmakoff is acknowledged for sharing experimental data.

REFERENCES

- (1) Hamm, P.; Lim, M. H.; Hochstrasser, R. M. Structure of the Amide I Band of Peptides Measured by Femtosecond Nonlinear Infrared Spectroscopy. *J. Phys. Chem. B* **1998**, *102*, 6123–6138.
- (2) Hamm, P.; Zanni, M. T. *Concepts and Methods of 2D Infrared Spectroscopy*; Cambridge University Press: Cambridge, U.K., 2011.
- (3) Woutersen, S.; Hamm, P. Time-Resolved Two-Dimensional Vibrational Spectroscopy of a Short α -Helix in Water. *J. Chem. Phys.* **2001**, *115*, 7737–7743.
- (4) Maekawa, H.; Toniolo, C.; Moretto, A.; Broxterman, Q. B.; Ge, N.-H. Different Spectral Signatures of Octapeptide 3₁₀- and α -Helices Revealed by Two-Dimensional Infrared Spectroscopy. *J. Phys. Chem. B* **2006**, *110*, 5835–5837.
- (5) Cheatum, C. M.; Tokmakoff, A.; Knoester, J. Signatures of β -Sheet Secondary Structures in Linear and Two-Dimensional Infrared Spectroscopy. *J. Chem. Phys.* **2004**, *120*, 8201–8215.
- (6) Woutersen, S.; Hamm, P. Isotope-Edited Two-Dimensional Vibrational Spectroscopy of Alanine in Aqueous Solution. *J. Chem. Phys.* **2001**, *114*, 2727–2737.
- (7) Manor, J.; Mukherjee, P.; Lin, Y.-S.; Leonov, H.; Skinner, J. L.; Zanni, M. T.; Arkin, I. T. Gating Mechanism of the Influenza A M2 Channel Revealed by 1D and 2D IR Spectroscopies. *Structure* **2009**, *17*, 247–254.
- (8) Moran, S. D.; Woys, A. M.; Buchanan, L. E.; Bixby, E.; Decatur, S. M.; Zanni, M. T. Two-Dimensional IR Spectroscopy and Segmental ¹³C Labeling Reveals the Domain Structure of Human γ D-Crystallin Amyloid Fibrils. *Proc. Nat. Acad. Sci. U.S.A.* **2012**, *109*, 3329–3334.
- (9) Lessing, J.; Roy, S.; Reppert, M.; Baer, M. D.; Marx, D.; Jansen, T. I. C.; Knoester, J.; Tokmakoff, A. Identifying Residual Structure in Intrinsically Disordered Systems: A 2D IR Spectroscopic Study of the GVGXPGVG Peptide. *J. Am. Chem. Soc.* **2012**, *134*, 5032–5035.
- (10) Smith, A. W.; Lessing, J.; Ganim, Z.; Peng, C. S.; Tokmakoff, A.; Roy, S.; Jansen, T. I. C.; Knoester, J. Melting of a β -Hairpin using Isotope Label-Edited 2D IR Spectroscopy and Simulations. *J. Phys. Chem. B* **2010**, *114*, 10913–10924.
- (11) Wang, J.; Chen, J.; Hochstrasser, R. M. Local Structure of β -Hairpin Isotopomers by FTIR, 2D IR, and Ab Initio Theory. *J. Phys. Chem. B* **2006**, *110*, 7545–7555.
- (12) Wang, J.; Zhuang, W.; Mukamel, S.; Hochstrasser, R. M. Two-Dimensional Infrared Spectroscopy as a Probe of the Solvent Electrostatic Field for a Twelve Residue Peptide. *J. Phys. Chem. B* **2008**, *112*, 5930–5937.

- (13) Roy, S.; Jansen, T. I. C.; Knoester, J. Structural Classification of the Amide I Sites of a β -Hairpin with Isotope Label 2DIR Spectroscopy. *Phys. Chem. Chem. Phys.* **2010**, *12*, 9347–9357.
- (14) Andresen, E. R.; Hamm, P. Site-Specific Difference 2D-IR Spectroscopy of Bacteriorhodopsin. *J. Phys. Chem. B* **2009**, *113*, 6520–6527.
- (15) Mu, Y.; Kosov, D. S.; Stock, G. Conformational Dynamics of Trialanine in Water. 2. Comparison of AMBER, CHARMM, GROMOS, and OPLS Force Fields to NMR and Infrared Experiments. *J. Phys. Chem. B* **2003**, *107*, 5064–5073.
- (16) Wang, L.; Middleton, C. T.; Zanni, M. T.; Skinner, J. L. Development and Validation of Transferable Amide I Vibrational Frequency Maps for Peptides. *J. Phys. Chem. B* **2011**, *115*, 3713–3724.
- (17) DeCamp, M. F.; DeFlores, L.; McCracken, J. M.; Tokmakoff, A.; Kwac, K.; Cho, M. Amide I Vibrational Dynamics of *N*-Methylacetamide in Polar Solvents: The role of Electrostatic Interactions. *J. Phys. Chem. B* **2005**, *109*, 11016–11026.
- (18) Jansen, T. I. C.; Knoester, J. A Transferable Electrostatic Map for Solvation Effects on Amide I Vibrations and its Application to Linear and Two-Dimensional Spectroscopy. *J. Chem. Phys.* **2006**, *124*, 044502.
- (19) Beauchamp, K. A.; Lin, Y.-S.; Das, R.; Pande, V. S. Are Protein Force Fields Getting Better? A Systematic Benchmark on 524 Diverse NMR Measurements. *J. Chem. Theory Comput.* **2012**, *8*, 1409–1414.
- (20) Jensen, F. *Introduction to Computational Chemistry*; Wiley & Sons: Chichester, U.K., 1999.
- (21) Guvench, O.; Mackerell, A. D. Comparison of Protein Force Fields for Molecular Dynamics Simulations. *Methods Mol. Biol. (Totowa, NJ, U. S.)* **2008**, *443*, 63–88.
- (22) Allen, M. P.; Tildesley, D. J. *Computer Simulation of Liquids*; Oxford University Press: Oxford, U.K., 1987.
- (23) Jorgensen, W. L.; Briggs, J. M.; Contreras, M. L. Relative Partition Coefficients for Organic Solutes from Fluid Simulations. *J. Phys. Chem.* **1990**, *94*, 1683–1686.
- (24) Jorgensen, W. L.; Chandrasekhar, J.; Madura, J. D.; Impey, R. W.; Klein, M. L. Comparison of Simple Potential Functions for Simulating Liquid Water. *J. Chem. Phys.* **1983**, *79*, 926–935.
- (25) Berendsen, H. J. C.; Grigera, J. R.; Straatsma, T. P. The Missing Term in Effective Pair Potentials. *J. Phys. Chem.* **1987**, *91*, 6269–6271.
- (26) Chang, T.-M.; Dang, L. X.; Peterson, K. A. Computer Simulation of Chloroform with a Polarizable Potential Model. *J. Phys. Chem. B* **1997**, *101*, 3413–3419.
- (27) Lamoureux, G.; Faraldo-Gomez, J. D.; Krupin, S.; Noskov, S. Y. Polarizable Model of Chloroform Based on Classical Drude Oscillators. *Chem. Phys. Lett.* **2009**, *468*, 270–274.
- (28) Jorgensen, W. L.; Schyman, P. Treatment of Halogen Bonding in the OPLS-AA Force Field: Application to Potent Anti-HIV Agents. *J. Chem. Theory Comput.* **2012**, *8*, 3895–3901.
- (29) Torii, H. Atomic Quadrupolar Effect in Intermolecular Electrostatic Interactions of Chloroalkanes: The Cases of Chloroform and Dichloromethane. *J. Mol. Liq.* **2005**, *119*, 31–39.
- (30) Auffinger, P.; Hays, F. A.; Westhof, E.; Ho, P. S. Halogen Bonds in Biological Molecules. *Proc. Natl. Acad. Sci. U.S.A.* **2004**, *101*, 16789–16794.
- (31) Metrangola, P.; Neukirch, H.; Pilati, T.; Resnati, G. Halogen Bonding Based Recognition Processes: A World Parallel to Hydrogen Bonding. *Acc. Chem. Res.* **2005**, *38*, 386–395.
- (32) Choi, J. H.; Ham, S. Y.; Cho, M. Local Amide I Mode Frequencies and Coupling Constants in Polypeptides. *J. Phys. Chem. B* **2003**, *107*, 9132–9138.
- (33) Watson, T. M.; Hirst, J. D. Influence of Electrostatic Environment of the Vibrational Frequencies of Proteins. *J. Phys. Chem. A* **2003**, *107*, 6843–6849.
- (34) Schmidt, J. R.; Corcelli, S. A.; Skinner, J. L. Ultrafast Vibrational Spectroscopy of Water and Aqueous *N*-Methylacetamide: Comparison of Different Electronic Structure/Molecular Dynamics Approaches. *J. Chem. Phys.* **2004**, *121*, 8887–8896.
- (35) Reppert, M.; Tokmakoff, A. Electrostatic Frequency Shifts in Amide I Vibrational Spectra: Direct Parameterization Against Experiment. *J. Chem. Phys.* **2013**, *138*, 134116.
- (36) Lin, Y.-S.; Shorb, J. M.; Mukherjee, P.; Zanni, M. T.; Skinner, J. L. Empirical Amide I Vibrational Frequency Map: Application to 2D-IR Line Shapes for Isotope-Edited Membrane Peptide Bundles. *J. Phys. Chem. B* **2009**, *113*, 592–602.
- (37) Hayashi, T.; Zhuang, W.; Mukamel, S. Electrostatic DFT Map for the Complete Vibrational Amide Band of NMA. *J. Phys. Chem. A* **2005**, *109*, 9747–9459.
- (38) Roy, S.; Lessing, J.; Meisl, G.; Ganim, Z.; Tokmakoff, A.; Knoester, J.; Jansen, T. I. C. Solvent and Conformation Dependence of Amide I Vibrations in Peptides and Proteins Containing Proline. *J. Chem. Phys.* **2011**, *135*, 234507.
- (39) Li, S.; Schmidt, J. R.; Corcelli, S. A.; Lawrence, C. P.; Skinner, J. L. Approaches for the Calculation of Vibrational Frequencies in Liquids: Comparisons to Benchmarks for Azide/Water Clusters. *J. Chem. Phys.* **2006**, *124*, 204110.
- (40) Hahn, E. L. Spin Echoes. *Phys. Rev.* **1950**, *80*, 580–594.
- (41) Roberts, S. T.; Loparo, J. J.; Tokmakoff, A. Characterization of Spectral Diffusion from Two-Dimensional Line Shapes. *J. Chem. Phys.* **2006**, *125*, 084502.
- (42) Cahoon, J. F.; Sawyer, K. R.; Schlegel, J. P.; Harris, C. B. Determining Transition-State Geometries in Liquids using 2D-IR. *Science* **2008**, *319*, 1820–1823.
- (43) Fecko, C. J.; Eaves, J. D.; Loparo, J. J.; Tokmakoff, A.; Geissler, P. L. Ultrafast Hydrogen-Bond Dynamics in the Infrared Spectroscopy of Water. *Science* **2003**, *301*, 1698–1702.
- (44) Zheng, J.; Kwak, K.; Asbury, J. B.; Chen, X.; Piletic, I. R.; Fayer, M. D. Ultrafast Dynamics of Solute-Solvent Complexation Observed at Thermal Equilibrium in Real Time. *Science* **2005**, *309*, 1338–1343.
- (45) Jansen, T. I. C.; Knoester, J. Calculation of Two-Dimensional Infrared Spectra of Ultrafast Chemical Exchange with Numerical Langevin Simulations. *J. Chem. Phys.* **2007**, *127*, 234502.
- (46) Bredenbeck, J.; Helbing, J.; Nienhaus, G. U.; Hamm, P. Protein Ligand Migration Mapped by Nonequilibrium 2D-IR Exchange Spectroscopy. *Proc. Nat. Acad. Sci. U.S.A.* **2007**, *104*, 14243–14248.
- (47) Hamm, P.; Helbing, J.; Bredenbeck, J. Two-Dimensional Infrared Spectroscopy of Photoswitchable Peptides. *Annu. Rev. Phys. Chem.* **2008**, *59*, 291–317.
- (48) King, J. T.; Baiz, C. R.; Kubarych, K. J. Solvent-Dependent Spectral Diffusion in Hydrogen Bonded “Vibrational Aggregate”. *J. Phys. Chem. A* **2010**, *114*, 10590–10604.
- (49) Schmidt, J. R.; Roberts, S. T.; Loparo, J. J.; Tokmakoff, A.; Fayer, M. D.; Skinner, J. L. Are Water Simulation Models Consistent with Steady-State and Ultrafast Vibrational Spectroscopy Experiments? *Chem. Phys.* **2007**, *341*, 143–157.
- (50) Brookes, J. F.; Slenkamp, K. M.; Lunch, M. S.; Khalil, M. Effect of Solvent Polarity on the Vibrational Dephasing Dynamics of the Nitrosyl Stretch in an Fe^{II} Complex Revealed by 2D IR Spectroscopy. *J. Phys. Chem. A* **2013**, *117*, 6234–6243.
- (51) Woutersen, S.; Mu, Y.; Stock, G.; Hamm, P. Hydrogen-Bond Lifetime Measured by Time-Resolved 2D-IR Spectroscopy: *N*-Methylacetamide in Methanol. *Chem. Phys.* **2001**, *266*, 137–147.
- (52) van Gunsteren, W. F.; Berendsen, H. J. C. Gromos-87 Manual. 1987.
- (53) Mark, A. E.; van Helden, S. P.; Janssen, P. E.; van Gunsteren, W. F. Convergence Properties of Free Energy Calculations: α -Cyclodextrin Complexes as a Case Study. *J. Am. Chem. Soc.* **1994**, *116*, 6293–6302.
- (54) van Buuren, A. R.; Marrink, S. J.; Berendsen, H. J. C. A Molecular Dynamics Study of the Decane/Water Interface. *J. Phys. Chem.* **1993**, *97*, 9206–9212.
- (55) Singh, U. C.; Kollman, P. A. An Approach to Computing Electrostatic Charges for Molecules. *J. Comput. Chem.* **1984**, *5*, 129–145.
- (56) Neese, F. The ORCA program system. *Wiley Interdiscip. Rev.: Comput. Mol. Sci.* **2012**, *2*, 73–78.

- (57) Perdew, J. P.; Burke, K.; Ernzerhof, M. Generalized Gradient Approximation Made Simple. *Phys. Rev. Lett.* **1996**, *77*, 3865–3668.
- (58) Schäfer, A.; Horn, H.; Ahlrichs, R. Fully Optimized Contracted Gaussian-Basis Sets for Atoms Li to Kr. *J. Chem. Phys.* **1992**, *97*, 2571–2577.
- (59) van Maaren, P. J.; van der Spoel, D. Molecular Dynamics Simulations of Water with Novel Shell-Model Potentials. *J. Phys. Chem. B* **2001**, *105*, 2618–2626.
- (60) Swart, M.; van Duijnen, P. T.; Snijders, J. G. Mean Polarizabilities of Organic Molecules. A Comparison of Restricted Hartree Fock, Density Functional Theory and Direct Reaction Field Results. *J. Mol. Struct.: THEOCHEM* **1999**, *458*, 11–17.
- (61) Essmann, U.; Perera, L.; Berkowitz, M. L.; Darden, T.; Lee, H.; Pedersen, L. G. A Smooth Particle Mesh Ewald Method. *J. Chem. Phys.* **1995**, *103*, 8577–8593.
- (62) Hoover, W. G. Canonical Dynamics: Equilibrium Phase-Space Distributions. *Phys. Rev. A* **1985**, *31*, 1695–1697.
- (63) Parrinello, M.; Rahman, A. Crystal Structure and Pair Potentials: A Molecular-Dynamics Study. *Phys. Rev. Lett.* **1980**, *45*, 1196–1199.
- (64) Hess, B.; Bekker, H.; Berendsen, H. J. C.; Fraaije, J. G. E. M. LINCS: A Linear Constraint Solver for Molecular Simulations. *J. Comput. Chem.* **1997**, *18*, 1463–1472.
- (65) Jansen, T. L. C.; Auer, B. M.; Yang, M.; Skinner, J. L. Two-Dimensional Infrared Spectroscopy and Ultrafast Anisotropy Decay of Water. *J. Chem. Phys.* **2010**, *132*, 224503.
- (66) Jansen, T. L. C.; Knoester, J. Waiting Time Dynamics in Two-Dimensional Infrared Spectroscopy. *Acc. Chem. Res.* **2009**, *42*, 1405–1411.
- (67) Torii, H. Time-Domain Calculations of the Polarized Raman and Two-Dimensional Infrared Spectra of Liquid *N,N*-Dimethylformamide. *Chem. Phys. Lett.* **2005**, *414*, 417–422.
- (68) Mukamel, S. *Principles of Nonlinear Optical Spectroscopy*; Oxford University Press: New York, 1995.
- (69) Jansen, T. L. C.; Knoester, J. Nonadiabatic Effects in the Two-Dimensional Infrared Spectra of Peptides: Alanine Dipeptide. *J. Phys. Chem. B* **2006**, *110*, 22910–22916.
- (70) Liang, C.; Jansen, T. L. C. An Efficient N^3 -Scaling Propagation Scheme for Simulating Two-Dimensional Infrared and Visible Spectra. *J. Chem. Theory Comput.* **2012**, *8*, 1706–1713.
- (71) Kwac, K.; Lee, H.; Cho, M. Non-Gaussian Statistics of Amide I Mode Frequency Fluctuations of *N*-Methylamide in Methanol Solution: Linear and Nonlinear Vibrational Spectra. *J. Chem. Phys.* **2004**, *120*, 1477–1490.
- (72) Hochstrasser, R. M. Two-Dimensional IR-Spectroscopy: Polarization Anisotropy Effects. *Chem. Phys.* **2001**, *266*, 273–284.
- (73) Lin, Y.-S.; Pieniazek, P. A.; Yang, M.; Skinner, J. L. On the Calculation of Rotational Anisotropy Decay, as Measured by Ultrafast Polarization-Resolved Vibrational Pump-Probe Experiments. *J. Chem. Phys.* **2010**, *132*, 174505.
- (74) Woutersen, S.; Bakker, H. J. Resonant Intermolecular Transfer of Vibrational Energy in Liquid Water. *Nature* **1999**, *402*, 507–509.
- (75) Møller, K. B.; Rey, R.; Hynes, J. T. Hydrogen Bond Dynamics in Water and Ultrafast Infrared Spectroscopy: A Theoretical Study. *J. Phys. Chem. A* **2004**, *108*, 1275–1289.
- (76) Hayashi, T.; Jansen, T. L. C.; Zhuang, W.; Mukamel, S. Collective Solvent Coordinates for the Infrared Spectrum of HOD in D_2O Based on an Ab Initio Electrostatic Map. *J. Phys. Chem. A* **2005**, *109*, 64–82.
- (77) Jansen, T. L. C.; Hayashi, T.; Zhuang, W.; Mukamel, S. Stochastic Liouville Equations for Hydrogen-Bonding Fluctuations and Their Signatures in Two-Dimensional Vibrational Spectroscopy of Water. *J. Chem. Phys.* **2005**, *123*, 114504.
- (78) Malolepsza, E.; Straub, J. E. Empirical Maps for the Calculation of Amide I Vibrational Spectra of Proteins from Classical Molecular Dynamics. *J. Phys. Chem. B* **2014**, DOI: 10.1021/jp412827s.
- (79) Cai, K.; Han, C.; Wang, J. Molecular Mechanics Force Field-Based Map for Peptide Amide-I Mode in Solution and its Application to Alanine Di- and Tripeptides. *Phys. Chem. Chem. Phys.* **2009**, *11*, 9149–9159.
- (80) Ham, S.; Kim, J. H.; Lee, H.; Cho, M. H. Correlation Between Electronic and Molecular Structure Distortions and Vibrational Properties. II. Amide I Modes of NMA- nD_2O Complexes. *J. Chem. Phys.* **2003**, *118*, 3491–3498.
- (81) Torii, H. Intra- and Intermolecular Charge Fluxes Induced by the OH stretching Mode of Water and Their Effects on the Infrared Intensities and Intermolecular Vibrational Coupling. *J. Phys. Chem. B* **2010**, *114*, 13404–13409.
- (82) Ottiger, P.; Pfaffen, C.; Leist, R.; Leutwyler, S.; Bachorz, R. A.; Kloppe, W. Strong $N-H\cdots\pi$ Hydrogen Bonding in Amide–Benzene Interactions. *J. Phys. Chem. B* **2009**, *113*, 2937–2943.
- (83) Humphrey, W.; Dalke, A.; Schulten, K. VMD: Visual Molecular Dynamics. *J. Mol. Graphics* **1996**, *14*, 33–38.
- (84) Sanni, S. A.; Hutchison, P. Diffusivities and Densities for Binary Liquid Mixtures. *J. Chem. Eng. Data* **1973**, *18*, 317–322.